Finite-size effect on the percolation and electromechanical behaviors of liquid metal particulate composites

Mohammad Madadi, Pu Zhang[1]

Department of Mechanical Engineering, State University of New York at Binghamton, Binghamton, NY 13902, United States

Abstract

Liquid metal particulate composites (LMPCs) are super-stretchable conductors with promising applications in soft electronics. Their conductance originates from the percolation networks of liquid metal particles. This work aims at elucidating the effect of finite-size and sample shape on the percolation and electromechanical properties of LMPCs, given that their dimensions range from microns to centimeters. It is found that their percolation threshold is dominated by the smallest dimension of the samples, not the shape or aspect ratio. A smaller sample size increases the percolation threshold and makes it harder to activate the conductance. In addition, smaller samples are more sensitive to local defects, which adversely impair the electromechanical properties or even undermine the conductance. Finally, this work considers the influence of finite-size on the piezoresistance effect, i.e., strain-dependent resistance. It is found that the piezoresistance effect and finite-size effect are uncorrelated, if the samples are above the percolation threshold. The findings provide not only fundamental insights on the finite-size effect of percolation but also guidance on the design-fabrication process for LMPCs to achieve more reliable electromechanical performance.

Keywords: Electromechanical behavior; Percolation; Size effect; Liquid metal composite

1 Introduction

There has been a strong demand for soft conductive materials that maintain high electrical conductivity under large and cyclic stretch for applications in soft electronics, soft robotics, and stretchable sensors [1–3]. Developing such conductive materials requires not only identifying material compositions and microstructures that offer desirable electromechanical properties but also deep understanding of the underlying mechanisms that govern conductivity under large strain. For a long time, researchers have focused on soft/flexible conductive composites embedded with highly conductive hard fillers such as carbon- and silver-based nano-materials [2,3]. Unfortunately, these hard fillers inevitably cause limited stretchability of the soft composites under

[1] Corresponding author. Email: pzhang@binghamton.edu

cyclic loading due to the rigidity-mismatch between the soft matrix and hard inclusions. To overcome this issue, researchers have recently developed soft conductive composites embedded with conductive liquid fillers [4,5], including liquid metal (LM) and electrolytes, to achieve superb stretchability and high conductivity simultaneously. Moreover, hybrid filler-based conductive composites [6] are also developed to exploit synergy advantages of hard and liquid fillers for optimal conductance and stretchability.

Among soft conductive composites with liquid fillers, liquid metal particulate composites (LMPCs) [7–10] are the most popular and promising ones because of their relatively high conductivity and facile synthesis process. In the literature, LMPCs are also called liquid metal embedded elastomers (LMEEs) [11]. Bulk LMs are very nasty to use directly due to their fluidic nature and enormous surface tension, usually ten times higher than water [12,13]. The easiest way to encapsulate and stabilize liquid metal is to embed it into an elastomer as particles or droplets [9,10]. So far, this process is matured and various methods have been developed to synthesize LMPC emulsions with particle sizes between tens of nanometers to microns [8,9,14]. Further, these LMPC emulsions can form different shapes using molding, screen printing, spin-coating, 3D printing, wet spinning, and electrospinning [15–17]. Potential applications of LMPCs have been reported for soft electronics, soft robotics, sensing, actuation, and electromagnetic shielding [1,10,18].

An unfavorable feature of LMPCs is that they are electrically insulated upon synthesis due to the native surface oxide surrounding LM particles. A subsequent mechanical sintering process [7,19] is usually necessary to activate the conductance. More specifically, mechanical pressure is applied on LMPCs so that the LM particles can break and form percolation networks in the composite. Other activation methods include freezing [20], laser sintering [21], and sonication [22], although mechanical sintering is still the most convenient and effective method. All these methods aim at realizing percolation of LM particles. There is no in-situ experimental observation on how the percolation process happens at the microscale. But researchers have tried to use numerical simulation to provide more insights. Cohen and Bhattacharya [23] performed finite element analysis (FEA) for a representative volume element (RVE) of LMPCs containing one or few particles. They found that the hydrostatic pressure in the deformed LM particles induces large tensile stress in the elastomer matrix, which may lead to crack initiation and propagation. Consequently, once LM flows into these microcracks, a conductive percolation network can be formed. To date, there is no simulation on the crack propagation and percolation network formation process yet. But researchers have attempted to study the electromechanical behaviors of LMPCs after percolation. One abnormal phenomenon of LMPCs is that their electrical resistance is strain-insensitive. Zolfaghari et al. [24] offered an explanation by studying the electromechanical properties of LMPCs with various network topologies and concluded that a tortuous percolation network results in the strain-insensitive resistance. In a following work [25]

from the same group, they studied the stochastic nature of the percolation network and the effect of percolation probability on the resistance of LMPCs.

The electromechanical properties of LMPCs are dominated by the connectivity of percolation networks [24,25]. In percolation theory, the percolation threshold shows some finite-size effect [26–28], namely, a smaller sample size usually has a higher percolation threshold given the same particle sizes. As shown in Figure 1, the LMPCs reported in the literature [11,17,29,30] exhibit various shapes and sizes, ranging from microns to centimeters. In particular, the structures in Figure 1 b-d only have ten or more LM particles along at least one dimension. In such cases, the connectivity of the percolation network is crucial to the electromechanical properties of the samples. Based on our experience with LMPC fibers [17], thicker fibers are usually easier to be electrically activated by mechanical sintering while thinner fibers are more challenging to do, which evidences some percolation size effect. So far, there is still poor understanding on the effect of finite-size on the percolation and electromechanical behaviors of LMPCs. In addition, percolation is not only influenced by the sample size but also the sample shape, and the latter is rarely studied in the literature. Hence, this work aims to fill this knowledge gap and elucidate the effect of finite-size and sample shape on the percolation and electromechanical behaviors of LMPCs. To achieve this aim, we perform FEA for LMPC composites with rectangular shapes and different sizes. In addition, we also study the roles of local defects and mechanical stretch on the electromechanical behaviors of LMPCs. This work will provide more fundamental insights on the percolation and electromechanical behaviors of LMPCs and soft conductive composites in general. Note that the finite-size effect is different from the particle-size effect. In experiment, it is harder to induce percolation when the LM particles shrink from microns to nanometers due to the surface oxides [14]. In this work, we focus on the percolation behavior of a LM network, not how the percolation is formed.

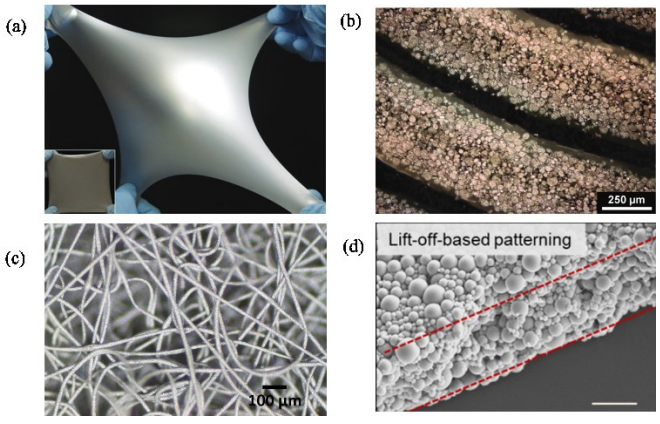

Figure 1 LMPCs reported in the literature exhibit various shapes and sizes ranging from microns to centimeters. (a) A thin film around 4 cm wide and a few mm thick [11], (b) 3D printed traces around 400 µm wide [30], (c) Electrospun fibers [17] around 20 µm thick fabricated in the authors'

lab, and (d) A thin film around 10 μm thick [29]. (Graphs are adapted from the references with permission.)

2 Computational modeling

2.1 The simulation model

It is impractical to simulate a large amount of LMPC models commensurate with experimental samples [7,17,29,30]. In experiment, LMPCs usually contain randomly distributed LM particles with varying diameters. After mechanical sintering, the LM particles percolate to each other but the detailed morphology of percolated networks is still unclear from the literature. Considering the stochastic nature of particle distributions and percolated networks, 3D FEA simulations will be computational costly. Thus, in this work, we consider an ideal composite network model in 2D to discover the effects of sample size and shape on the percolation and electromechanical properties. Note that the simulation results will offer only qualitative rather than quantitative analysis for LMPCs.

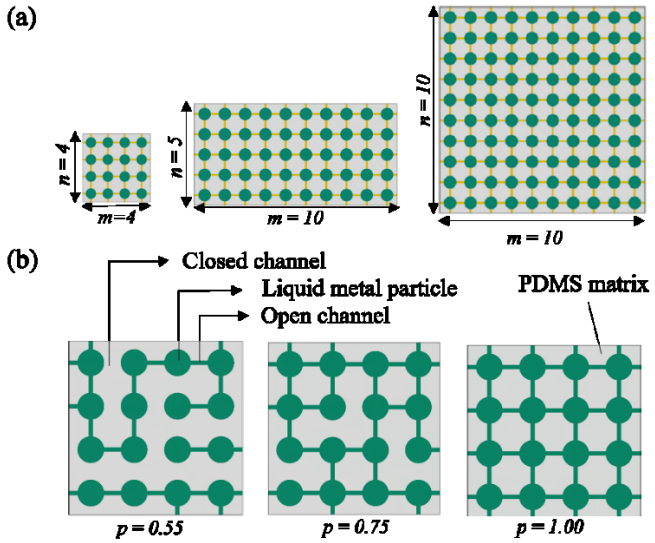

Figure 2 Schematic illustrations of the 2D composite samples simulated in this work. (a) Square and rectangular samples with different sizes and aspect ratios. Each unit cell consists of one LM particle and four channels connecting neighbor unit cells. (b) Representative percolation networks for specific percolation probability p. The open channels are electrically conductive and closed channels are insulated. The open/closed channels are distributed randomly to capture the stochastic nature of the percolation network.

As illustrated in Figure 2a, we consider 2D rectangular models consisting of *m* unit cells in length and *n* unit cells in width. Each unit cell is square shaped with an edge length of 10 μm. A unit cell consists of a circular LM particle in the center and four thin channels connecting neighbor unit cells. Considering a volume fraction of 30 vol% for LM, the diameter of LM particles is about 6.18 μm and the channel width is 1 μm. In addition, the thickness of the 2D composite models is set as 1 μm in all simulations. As illustrated in Figure 2b, selected channels are filled with LM to form a percolation network, mimicking the mechanical sintering process. It is noted that the percolation behavior is dictated by the percolation probability *p* instead of the volume fraction of LM. The volume fraction of LM only influences the magnitude of resistance but not the percolation transition. Certainly, it is usually easier to achieve a greater percolation probability in experiments if the volume fraction of LM is higher. The channels between LM particles are either open or closed: open channels are conductive while closed ones are insulated. The open and closed channels are distributed randomly once the percolation probability *p* of the whole model is given. Herein, the percolation probability *p* is defined as the ratio of open channels among all channels, and p=0 indicates no percolation while p=1 indicates fully-percolated. Usually, once the sample size (i.e., *m* and *n*) is set and percolation probability *p* is given, we will generate numerous simulation models randomly to consider the stochastic nature of the percolation network and extract the statistical electromechanical properties. By default, we generated 170 simulation models for each parameter set (m, n, p) unless otherwise specified. For a specific composite model, the FEA simulation is conducted using a commercial package ABAQUS (v2020, Dassault Systèmes). A representative FEA model and the mesh are shown in Figure S1 of the Supplementary Information.

2.2 Material models

The mechanical models used in the FEA are introduced first. Polydimethylsiloxane (PDMS) is the most popular matrix material for LMPCs in the literature. Hence, we choose PDMS as the soft matrix in our model. We do not specify the LM composition in our model. The most popular ones are $Ga_{75.5}In_{24.5}$ and $Ga_{68.5}In_{21.5}Sn_{10}$. Both the PDMS and LM phases are modeled as nearly incompressible neo-Hookean solids with a hyperelastic strain energy function [31] given as $W = 0.5\mu(\bar{I}_1 - 3) + 0.5\kappa(J-1)^2$, where μ, $\bar{I}_1$, κ, and J are the initial shear modulus, the first deviatoric invariant of strain, initial bulk modulus, and volumetric deformation, respectively. For both PDMS and LM, the bulk modulus is set as $\kappa = 50\mu$ to capture the incompressibility and reduce computational cost meanwhile. Although LM is a liquid, researchers usually model it as a soft solid with vanishing shear modulus [23]. In this work, the shear modulus of PDMS is $\mu^{PDMS} = 21.6$ KPa [32] and we choose a small shear modulus for LM, as $\mu^{LM} = 0.05\mu^{PDMS}$. Note that the computational cost will increase if even smaller shear modulus is set for LM. Table 1 exhibits the mechanical properties of the PDMS matrix and LM particles used in the FEA model.

Table 1 Material properties of PDMS and LM used for the simulations.

Material	μ (KPa)	κ (KPa)	σ_E (S/mm)
PDMS	21.6	1080	0.1
LM	1.08	54	3000

The electrical conductivity σ_E is needed for the two materials to study the electromechanical properties. A typical range of electrical conductivities for LMs is 3000-4000 S/mm [33]. Although the PDMS matrix is insulated, it is considered to have a minimal conductivity in the FEA model to avoid singularity of the electrical equations. Table 1 also exhibits the electrical conductivities used in our simulations.

Specifically, the material properties are assigned in the following manner. The matrix and particles are assigned as PDMS and LM, respectively. For the channels, we need to distinguish between open and closed channels. The closed channels are insulated so they are assigned as PDMS. For open channels, their electrical properties are taken as LM's but their mechanical properties are chosen as the same as PDMS. This particular setup will guarantee that the composite still has mechanical strength even if all channels are percolated.

2.3 Electromechanical modeling

Electromechanical simulations were performed for the FEA models shown in Figure 2 using ABAQUS. The computational procedure consists of a mechanical analysis step followed by an electrical analysis step similarly reported by Overvelde [34]. More specifically, the electrical analysis is performed on a pre-stretched model from the mechanical analysis step. The detailed analysis procedure is introduced below. For the mechanical analysis, the composite model is discretized by plane stress triangular elements CPS3. Uniaxial stretch deformation is imposed on the left and right edges of the model. The top and bottom edges of the model are free. The displacement fields of each frame are exported for the electrical analysis step. For the electrical analysis step (i.e., coupled thermal-electrical analysis in ABAQUS), the composite model is discretized by thermal-electrical triangular elements DC2D3E. Note that the mesh in the electrical analysis step is identical to that in the mechanical analysis step. A constant voltage drop is imposed on the left and right edges to induce a current flow; meanwhile the top and bottom edges are electrically insulated.

To obtain the electrical resistance of samples, a voltage V is imposed between the left and right edges of the model. The total Joule heating power U of the whole FEA model is extracted from ABAQUS directly. Finally, the electrical resistance R of the sample is given as $R = V^2/U$. Note that the resistance R depends on the mechanical deformation as well. So, for electromechanical behaviors, we need to compute the R for each frame of the mechanical analysis step.

3 Results and discussions

A few factors are studied in this section to uncover the effects of sample size and shape on the percolation and electromechanical properties of LMPCs. At first, we consider square and rectangular samples with various sizes, aspect ratios, and percolation probability. The effect of finite-size and shape on the percolation threshold will be introduced. Next, we consider the effect of local defects on the percolation and conductivity of rectangular samples. This analysis will be useful for the reliability design of LMPCs. Finally, the influence of mechanical stretch on the electromechanical behaviors is studied.

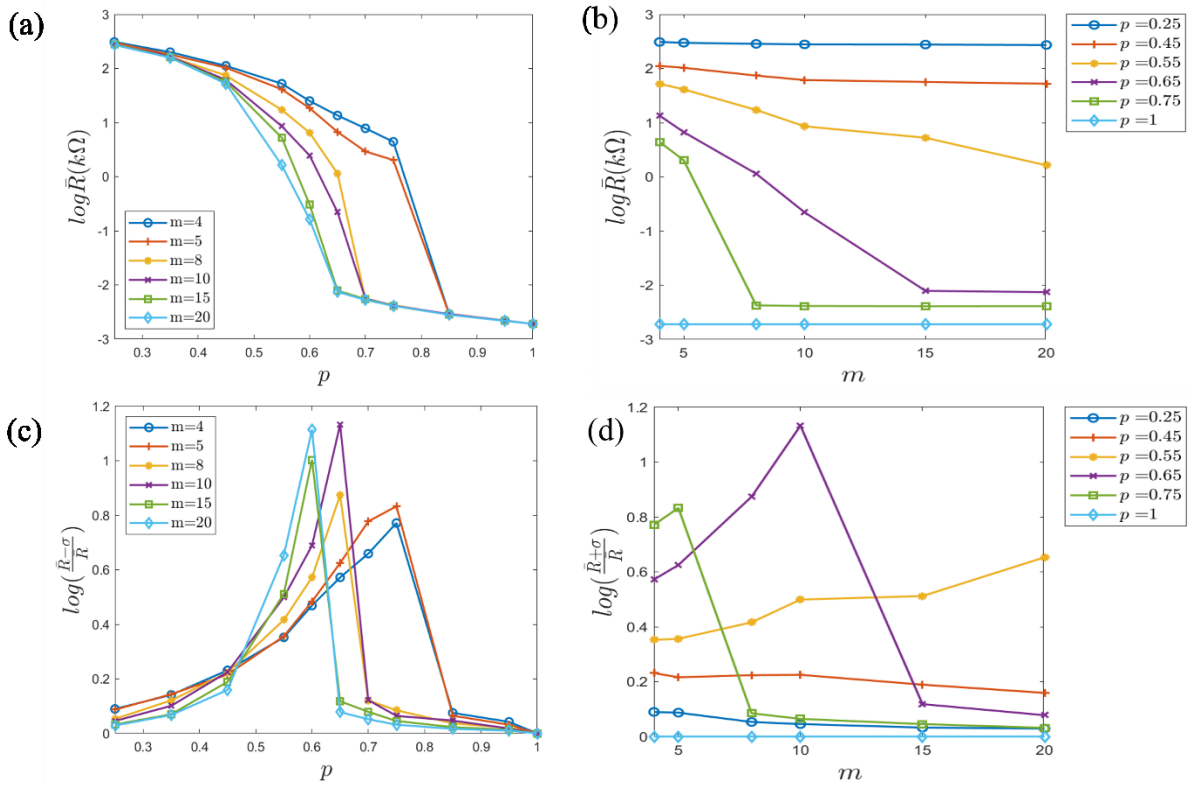

Figure 3 (a) Mean resistance versus percolation probability p for various sizes m of square samples. (b) Mean resistance versus m for different p. (c) Standard deviation of resistance versus

percolation probability p for various sizes of square samples. (d) Standard deviation of resistance versus m for different p.

3.1 Size effect

A square model with $m*m$ unit cells is considered first to uncover the finite-size effect of percolation for LMPCs. We first calculate the electrical resistance of 170 models for each parameter set (m, p). The resistance data is analyzed and plotted in Figure 3 in logarithmic scale. The raw data is also plotted in Figure S2. Figure 3a presents the mean resistance $\bar{R}$ for different sample sizes m and percolation probability p. The resistance shows a sudden drop as the percolation probability p increases across the percolation threshold. Meanwhile, the composite changes from an insulator to a conductor. For LMPCs, a lower percolation threshold means that the conductance can be activated easily by mechanical sintering. In contrast, a higher percolation threshold means that it is harder to activate the conductance. From Figure 3a, we find that the percolation threshold decreases when the sample size m is bigger. Herein we consider a wide range of sample sizes. The small model m=4 and big model m=20 almost correspond to the upper and lower bounds of the percolation threshold, respectively. Figure 3b shows the same set of data in an alternative way. The finite-size has a significant effect on the sample resistance when the percolation probability p is close to the percolation threshold. Considering the stochastic nature of the percolation network and resistance response, we also plot the standard deviation of resistance in Figure 3c-d. It is observed that the standard deviation peaks when the percolation probability is close to the percolation threshold. This phenomenon is easy to understand because that the resistance values of samples vary a lot around percolation, i.e., insulator-conductor transition. In summary, our results from the square models show that the sample size has a strong influence on the percolation threshold of LMPCs. When the sample size shrinks to only a few particles along one dimension, it is challenging to activate its conductance and achieve reliable electromechanical responses. Of course, the finite-size effect disappears when the unit cell number m is large enough. We found that this effect is almost negligible when $m \geq 14$.

3.2 Shape effect

As shown in Figure 1, most LMPCs have distinct feature sizes along different dimensions. For example, LMPC fibers in Figure 1c are extremely long but ultra-thin with only a dozen of particles along the diameter direction. The thin films in Figure 1d are wide in-plane but very thin along the thickness direction. How does the sample shape affect the percolation and electromechanical properties? We will address this question by performing simulations for rectangular samples with different sizes and aspect ratios. Herein, we consider both narrow (n=5) and wide (n=10) samples with four aspect ratios m/n. The results are presented in Figure 4 and raw data are also shown in Figures S3-S4.

Figure 4a-b show the mean resistance of rectangular samples with different aspect ratios and width. In theory, the resistance is proportional to the aspect ratio (i.e., $R \propto m/n$) and independent to the width n, which is confirmed in Figure 4a-b. Thus, the aspect ratio m/n of the rectangular samples does not affect the percolation threshold. By comparing Figure 4a and 4b, we found that the percolation threshold of the narrow samples (n=5) is much larger than the wide samples (n=10). In other words, a narrower sample is harder to be electrically activated or mechanically sintered, which is consistent to our findings when we process LMPC fibers. From Figure 4a-b, we conclude that the percolation threshold of rectangular samples is dictated by the smaller dimension, not the shape (or aspect ratio). In addition to the mean resistance, we also present the standard deviation of resistance in Figure 4c-d. Again, the standard deviation peaks around the percolation threshold. The comparison of standard deviations does not provide much useful information given that the mean resistance values replies on the aspect ratio m/n.

We can also speculate that for 3D LMPCs in general, the percolation threshold is dictated by the smallest dimension, not the shape or aspect ratio. If there are only a few tens of particles along one dimension, we will need to consider the finite-size effect on the percolation and electromechanical properties. This is crucially important to achieve reliable electromechanical performance when engineers design and fabricate LMPC-based devices.

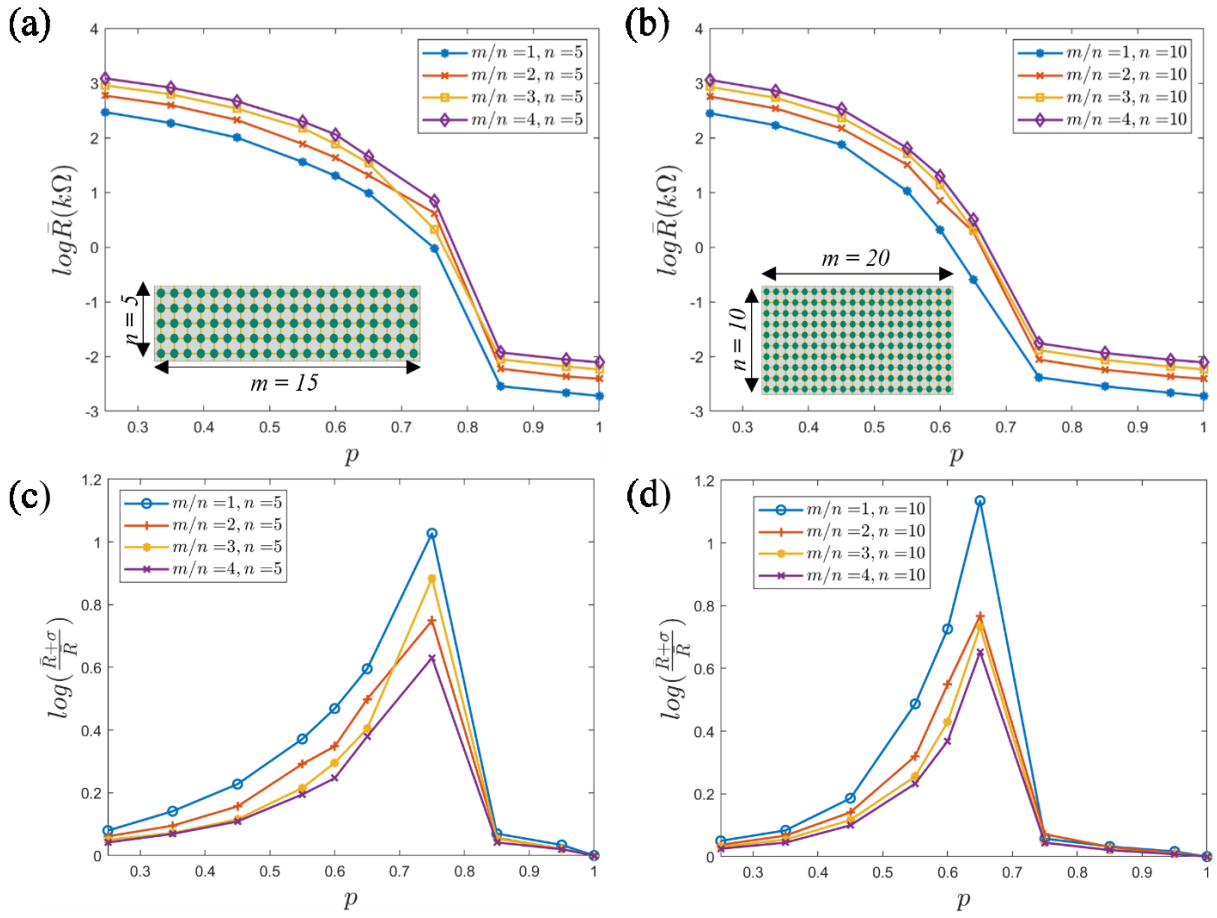

Figure 4 Mean resistance versus percolation probability p for rectangular samples with different aspect ratios: (a) n=5, (b) n=10. The corresponding standard deviation is shown in (c) n=5 and (d) n =10. The percolation threshold is dictated by the smaller dimension rather than the aspect ratio.

3.3 Effect of local defects

When a conductive network has finite-size, its resistance is not only related to the overall percolation probability but also the spatial variation of percolation, especially when local defects exist. Empirically, the effect of local defects is significant when the dimension is small along at least one direction. In practice, local defects exist in LMPCs either induced in the manufacturing process or incomplete mechanical sintering. For example, the LMPC fiber [17] in Figure 5a contains a defect region due to manufacturing defects. This local defect region impairs electromechanical properties of the LMPC samples. The adverse effect of local defects can be devastating when the samples are thin and long. In order to gain some insights on this phenomenon, we consider a rectangular model (40*10 unit cells) with a local defect region (4*10 unit cells) in the middle, as shown in Figure 5b. The two ends of this sample are highly conductive with a high percolation probability p=0.85 while the defect region has a lower percolation probability p_d=

0.25~0.85. We expect that when p_d increases from 0.25 to 0.85, the sample will transit from an insulator to a conductor, which is confirmed in Figure 5c from the mean resistance data. The standard deviation of resistance in Figure 5d peaks around the percolation threshold, similar to previous observations. Moreover, the length of the defect region also exhibits some finite-size effect. The percolation threshold of a defect region is lower when the defect region becomes longer. This study provides some guidance on the reliability design of LMPC components. Generally, when any dimension is small, e.g., for thin films or fibers, there is a large chance that any local defects will impair the electromechanical properties significantly, and efforts are needed to reduce local defects caused in the manufacturing and sintering processes. In contrary, when the dimension of the sample is large, it is easy to find percolation pathways and is less sensitive to local defects.

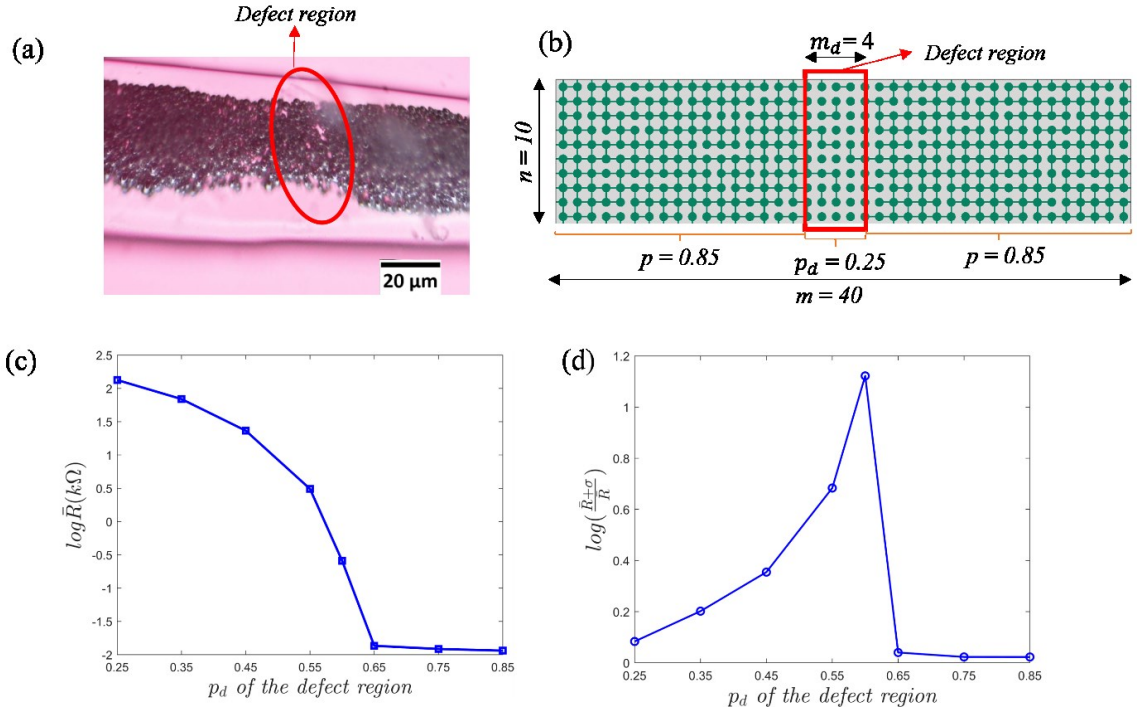

Figure 5 (a) Optical microscopy of a LM fiber with a defect region caused from manufacturing defects. The defect region will impair the electromechanical properties. (b) A simplified simulation model for a rectangular sample with a defect region. The percolation probability p_d of the defect region is lower than the rest of the sample p=0.85. (c) Mean resistance versus percolation probability p_d of the defect region. (d) Standard deviation of resistance versus percolation probability p_d of the defect region.

3.4 Effect of stretch

LMPCs are highly stretchable conductors due to the fluidic nature of LM (see Figure 6a). Generally, the resistance of a conductor is strain-dependent, which is also called the piezoresistance effect. The normalized resistance of an ideal conductor follows a Pouillet's law [24], $R/R_0 = \lambda^2$, with R_0 the initial resistance, R the resistance under stretch, and λ the stretch ratio. Surprisingly, the resistance of LMPCs is found to be insensitive to stretch [24]. Previous studies have attributed this abnormal phenomenon to possibly tortuous percolation pathways in LMPCs after mechanical sintering [24,25]. As shown in Figure 6b, under uniaxial stretch, the resistance increase of horizontal channels is compensated by the resistance decrease of vertical channels, which results in a strain-insensitive resistance in LMPCs [25]. Previous study [25] also found that the normalized resistance R/R_0 is less sensitive to the stretch ratio λ when the percolation probability *p* decreases, which is also confirmed by our simulation results in Figure 6d or Figure S6 for the case m=n=10.

There are still two fundamental questions yet to be answered. Firstly, does the piezoresistance (i.e., stretch-resistance) responses show a finite-size effect like percolation? Secondly, how does the standard deviation of normalized resistance change under stretch? To address the first question, we compared the normalized resistance R/R_0 of a 10*10 square model and a 5*5 square model for p=0.85 so both models are percolated. Herein we assume that the percolation probability keeps constant under stretch, although in practice it may increase. The comparison in Figure 6d shows that the stretch-resistance responses of two samples with different sizes are almost identical. This observation indicates that once the samples are percolated and become conductors, the finite-size has no influence on the piezoresistance response. In other words, above the percolation threshold, the finite-size effect and the piezoresistance effect are uncorrelated. To address the second question, we plot the standard deviation of normalized resistance in Figure 6e. We found that the finite-size effect does have an effect on the standard deviation of normalized resistance, given the fact that the smaller sample with 5*5 unit cells has much greater variance than the bigger sample with 10*10 unit cells. This effect implies that it is more challenging to obtain reliable electromechanical performance when the sample sizes are smaller. In addition to the finite-size effect, it is found that the standard deviation usually increases under stretch, implying larger variance of the piezoresistance responses. In addition, the standard deviation decreases once the percolation *p* increases, because *p* is further away from the percolation threshold, where the peak of standard deviation is. Although the results in Figure 6 are for samples with 30 vol% of LM, the findings still hold true for higher volume fractions. The electromechanical behaviors of LMPCs with 50 vol% are shown in Figure S7. It is confirmed that the volume fraction only influences the magnitude of the responses but not the general trends. The findings from Figure 6 have practical implications for the design-fabrication of LMPC sensors. For instance, to achieve high reliability

and accuracy for the piezoresistance responses, these LMPC sensors need to be better percolated, exhibit a relatively big size, and operate under an allowable stretch ratio.

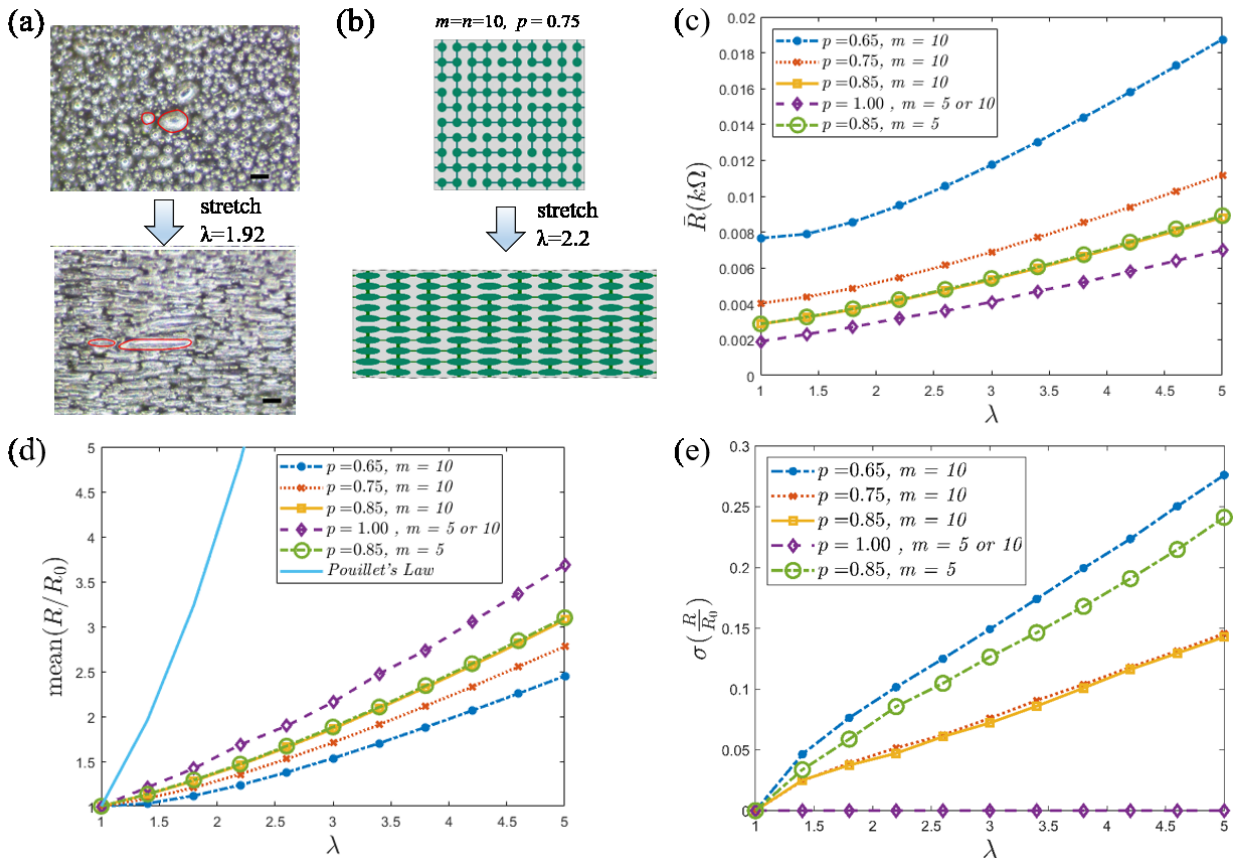

Figure 6 (a) Optical microscopy of a LMPC before and after stretch. The edges of two particles are highlighted to show the deformation. Scale bar is 20 μm. (b) A square sample with 10*10 unit cells before and after stretch. The percolation probability is p = 0.75. (c) Influence of the stretch ratio λ on the mean resistance. (d) Influence of the stretch ratio λ on the normalized resistance. The finite-size effect has no correlation with the stretch-resistance responses. (e) Influence of the stretch ratio λ on the standard deviation of the normalized resistance. A smaller sample size induces greater variance of the normalized resistance. Each data point is averaged from 50 simulation models.

4 Conclusions

LMPCs are super-stretchable conductors with promising applications in soft electronics, soft robotics, sensing, etc. Normally, LMPCs are insulated right after synthesis and an activation process is necessary to achieve conductance, e.g., employing mechanical sintering. The underlying principle of the activation process is to create percolation networks for the embedded LM particles.

The LMPCs reported in the literature have different dimensions ranging from microns to centimeters. In many cases, the LMPCs only have limited size along one or two dimensions. This brings up an issue to the percolation network due to the finite-size effect. This work aims at elucidating the effect of finite-size on the percolation and electromechanical properties of LMPCs. More specifically, we studied various factors such as the size, aspect ratio, local defects, and stretch. We discovered that the percolation threshold is mainly dominated by the smallest dimension of the sample, not the shape or aspect ratio. A smaller sample size will unfortunately increase the percolation threshold and make it harder to activate the conductance. In addition, the existence of local defects or incomplete percolation regions will adversely impair the electromechanical properties and sometimes undermine the conductance. Smaller samples are more sensitive to local defects. Finally, we also studied the influence of finite-size on the piezoresistance effect, i.e., strain-resistance relations. We discovered that the piezoresistance effect is not correlated to the finite-size effect, if the samples are above the percolation threshold. The findings in this work provide not only insights on the finite-size effect of percolation for LMPCs but also guidance on their design-fabrication process to achieve better and more reliable electromechanical performance for soft electronics applications.

Future research can be towards multiple directions. Firstly, there is still a knowledge gap on the experimental study for the reported finite-size effect of LMPCs. The technical challenge is that one needs to fabricate samples with precise sizes and design experiments to control the percolation probability through mechanical sintering. Secondly, the major findings from 2D models of this work are still valid for 3D LMPCs such as thin films [16,29]. But the detailed electromechanical responses and defect structures are more complicated and deem further simulation study. Thirdly, our work is limited to uniform particle distributions. Recent literature has reported LMPCs with non-uniform particle distributions induced by sedimentation [35–38]. The percolation and finite-size effect of these gradient microstructures are complicated, which require simulations using 3D realistic models.

Author contributions

MM: Conceptualization, Formal Analysis, Investigation, Methodology, Writing-original draft; PZ: Conceptualization, Formal Analysis, Methodology, Supervision, Writing-review & editing.

Acknowledgments

We acknowledge the funding support from National Science Foundation (CMMI-2143297).

References

[1] M.D. Dickey, Stretchable and Soft Electronics using Liquid Metals, Adv. Mater. 29 (2017) 1606425. https://doi.org/10.1002/adma.201606425.

[2] K. Sakuma, Flexible, Wearable, and Stretchable Electronics, 1st ed., CRC Press, First edition. | Boca Raton : CRC Press, 2020. | Series: Devices, circuits, & systems, 2020. https://doi.org/10.1201/9780429263941.

[3] S. Choi, S.I. Han, D. Kim, T. Hyeon, D.-H. Kim, High-performance stretchable conductive nanocomposites: materials, processes, and device applications, Chem. Soc. Rev. 48 (2019) 1566–1595. https://doi.org/10.1039/C8CS00706C.

[4] R.W. Style, R. Tutika, J.Y. Kim, M.D. Bartlett, Solid–Liquid Composites for Soft Multifunctional Materials, Adv. Funct. Mater. 31 (2021) 2005804. https://doi.org/10.1002/adfm.202005804.

[5] Z. Sheng, Y. Ding, G. Li, C. Fu, Y. Hou, J. Lyu, K. Zhang, X. Zhang, Solid–Liquid Host–Guest Composites: The Marriage of Porous Solids and Functional Liquids, Advanced Materials. 33 (2021) 2104851. https://doi.org/10.1002/adma.202104851.

[6] G. Yun, S.-Y. Tang, H. Lu, S. Zhang, M.D. Dickey, W. Li, Hybrid-Filler Stretchable Conductive Composites: From Fabrication to Application, Small Science. 1 (2021) 2000080. https://doi.org/10.1002/smsc.202000080.

[7] A. Fassler, C. Majidi, Liquid-Phase Metal Inclusions for a Conductive Polymer Composite, Adv. Mater. 27 (2015) 1928–1932. https://doi.org/10.1002/adma.201405256.

[8] R. Tutika, S. Kmiec, A.B.M.T. Haque, S.W. Martin, M.D. Bartlett, Liquid Metal–Elastomer Soft Composites with Independently Controllable and Highly Tunable Droplet Size and Volume Loading, ACS Appl. Mater. Interfaces. 11 (2019) 17873–17883. https://doi.org/10.1021/acsami.9b04569.

[9] N. Kazem, T. Hellebrekers, C. Majidi, Soft Multifunctional Composites and Emulsions with Liquid Metals, Adv. Mater. 29 (2017) 1605985. https://doi.org/10.1002/adma.201605985.

[10] S. Chen, H.-Z. Wang, R.-Q. Zhao, W. Rao, J. Liu, Liquid Metal Composites, Matter. 2 (2020) 1446–1480. https://doi.org/10.1016/j.matt.2020.03.016.

[11] M.D. Bartlett, N. Kazem, M.J. Powell-Palm, X. Huang, W. Sun, J.A. Malen, C. Majidi, High thermal conductivity in soft elastomers with elongated liquid metal inclusions, Proc Natl Acad Sci USA. 114 (2017) 2143–2148. https://doi.org/10.1073/pnas.1616377114.

[12] Z. Yang, D. Yang, X. Zhao, Q. Zhao, M. Zhu, Y. Liu, Y. Wang, W. Lu, D. Qi, From liquid metal to stretchable electronics: Overcoming the surface tension, Sci. China Mater. 65 (2022) 2072–2088. https://doi.org/10.1007/s40843-021-2023-x.

[13] Q. Xu, N. Oudalov, Q. Guo, H.M. Jaeger, E. Brown, Effect of oxidation on the mechanical properties of liquid gallium and eutectic gallium-indium, Physics of Fluids. 24 (2012) 063101. https://doi.org/10.1063/1.4724313.

[14] M.H. Malakooti, M.R. Bockstaller, K. Matyjaszewski, C. Majidi, Liquid metal nanocomposites, Nanoscale Adv. 2 (2020) 2668–2677. https://doi.org/10.1039/D0NA00148A.

[15] G.G. Guymon, M.H. Malakooti, Multifunctional liquid metal polymer composites, Journal of Polymer Science. 60 (2022) 1300–1327. https://doi.org/10.1002/pol.20210867.

[16] A.B.M. Tahidul Haque, R. Tutika, M. Gao, A. Martinez, J. Mills, J. Arul Clement, J. Gao, M. Tabrizi, M. Ravi Shankar, Q. Pei, M.D. Bartlett, Conductive liquid metal elastomer thin films with multifunctional electro-mechanical properties, Multifunct. Mater. 3 (2020) 044001. https://doi.org/10.1088/2399-7532/abbc66.

[17] J. Ma, Z. Liu, Q. Nguyen, P. Zhang, Lightweight Soft Conductive Composites Embedded with Liquid Metal Fiber Networks, Adv Funct Materials. (2023) 2308128. https://doi.org/10.1002/adfm.202308128.

[18] W. Babatain, M.S. Kim, M.M. Hussain, From Droplets to Devices: Recent Advances in Liquid Metal Droplet Enabled Electronics, Adv Funct Materials. (2023) 2308116. https://doi.org/10.1002/adfm.202308116.

[19] E.J. Markvicka, M.D. Bartlett, X. Huang, C. Majidi, An autonomously electrically self-healing liquid metal–elastomer composite for robust soft-matter robotics and electronics, Nature Mater. 17 (2018) 618–624. https://doi.org/10.1038/s41563-018-0084-7.

[20] L. Zhou, J. Fu, Q. Gao, P. Zhao, Y. He, All-Printed Flexible and Stretchable Electronics with Pressing or Freezing Activatable Liquid-Metal–Silicone Inks, Adv. Funct. Mater. 30 (2020) 1906683. https://doi.org/10.1002/adfm.201906683.

[21] M.G. Mohammed, R. Kramer, All-Printed Flexible and Stretchable Electronics, Adv. Mater. 29 (2017) 1604965. https://doi.org/10.1002/adma.201604965.

[22] W. Lee, H. Kim, I. Kang, H. Park, J. Jung, H. Lee, H. Park, J.S. Park, J.M. Yuk, S. Ryu, J.-W. Jeong, J. Kang, Universal assembly of liquid metal particles in polymers enables elastic printed circuit board, Science. 378 (2022) 637–641. https://doi.org/10.1126/science.abo6631.

[23] N. Cohen, K. Bhattacharya, A numerical study of the electromechanical response of liquid metal embedded elastomers, International Journal of Non-Linear Mechanics. 108 (2019) 81–86. https://doi.org/10.1016/j.ijnonlinmec.2018.10.011.

[24] N. Zolfaghari, P. Khandagale, M.J. Ford, K. Dayal, C. Majidi, Network topologies dictate electromechanical coupling in liquid metal–elastomer composites, Soft Matter. 16 (2020) 8818–8825. https://doi.org/10.1039/D0SM01094D.

[25] Y. Zhao, P. Khandagale, C. Majidi, Modeling electromechanical coupling of liquid metal embedded elastomers while accounting stochasticity in 3D percolation, Extreme Mechanics Letters. 48 (2021) 101443. https://doi.org/10.1016/j.eml.2021.101443.

[26] D. Stauffer, A. Aharony, Introduction To Percolation Theory, 0 ed., Taylor & Francis, 2018. https://doi.org/10.1201/9781315274386.

[27] A.-M.S. Tremblay, J. Machta, Finite-size effects in continuum percolation, Phys. Rev. B. 40 (1989) 5131–5139. https://doi.org/10.1103/PhysRevB.40.5131.

[28] M. Žeželj, I. Stanković, From percolating to dense random stick networks: Conductivity model investigation, Phys. Rev. B. 86 (2012) 134202. https://doi.org/10.1103/PhysRevB.86.134202.

[29] G.-H. Lee, H. Kim, J. Lee, J.-Y. Bae, C. Yang, H. Kim, H. Kang, S.Q. Choi, S. Park, S.-K. Kang, J. Kang, Z. Bao, J.-W. Jeong, S. Park, Large-area photo-patterning of initially conductive EGaIn particle-assembled film for soft electronics, Materials Today. 67 (2023) 84–94. https://doi.org/10.1016/j.mattod.2023.05.025.

[30] T.V. Neumann, E.G. Facchine, B. Leonardo, S. Khan, M.D. Dickey, Direct write printing of a self-encapsulating liquid metal–silicone composite, Soft Matter. 16 (2020) 6608–6618. https://doi.org/10.1039/D0SM00803F.

[31] G.A. Holzapfel, Nonlinear solid mechanics: a continuum approach for engineering, Wiley, Chichester ; New York, 2000.

[32] J.T.B. Overvelde, D.M.J. Dykstra, R. De Rooij, J. Weaver, K. Bertoldi, Tensile Instability in a Thick Elastic Body, Phys. Rev. Lett. 117 (2016) 094301. https://doi.org/10.1103/PhysRevLett.117.094301.

[33] S. Handschuh-Wang, F.J. Stadler, X. Zhou, Critical Review on the Physical Properties of Gallium-Based Liquid Metals and Selected Pathways for Their Alteration, J. Phys. Chem. C. 125 (2021) 20113–20142. https://doi.org/10.1021/acs.jpcc.1c05859.

[34] J.T.B. Overvelde, Y. Mengüç, P. Polygerinos, Y. Wang, Z. Wang, C.J. Walsh, R.J. Wood, K. Bertoldi, Mechanical and electrical numerical analysis of soft liquid-embedded deformation sensors analysis, Extreme Mechanics Letters. 1 (2014) 42–46. https://doi.org/10.1016/j.eml.2014.11.003.

[35] H. Wang, Y. Yao, Z. He, W. Rao, L. Hu, S. Chen, J. Lin, J. Gao, P. Zhang, X. Sun, X. Wang, Y. Cui, Q. Wang, S. Dong, G. Chen, J. Liu, A Highly Stretchable Liquid Metal Polymer as Reversible Transitional Insulator and Conductor, Adv. Mater. 31 (2019) 1901337. https://doi.org/10.1002/adma.201901337.

[36] A.B.M.T. Haque, D.H. Ho, D. Hwang, R. Tutika, C. Lee, M.D. Bartlett, Electrically Conductive Liquid Metal Composite Adhesives for Reversible Bonding of Soft Electronics, Adv Funct Materials. (2023) 2304101. https://doi.org/10.1002/adfm.202304101.

[37] J.-E. Park, H.S. Kang, J. Baek, T.H. Park, S. Oh, H. Lee, M. Koo, C. Park, Rewritable, Printable Conducting Liquid Metal Hydrogel, ACS Nano. 13 (2019) 9122–9130. https://doi.org/10.1021/acsnano.9b03405.

[38] P. Zhang, Q. Wang, R. Guo, M. Zhang, S. Wang, C. Lu, M. Xue, J. Fan, Z. He, W. Rao, Self-assembled ultrathin film of CNC/PVA–liquid metal composite as a multifunctional Janus material, Mater. Horiz. 6 (2019) 1643–1653. https://doi.org/10.1039/C9MH00280D.